

Geophysical data combination for a 3D model of the Mediterranean Sea: first results

M. CAPPONI¹, G. MAURIZIO² AND D. SAMPIETRO¹

¹ *Geomatics Research & Development S.r.l., Lomazzo (CO), Italy*

² *Dipartimento di Matematica e Geoscienze, Università degli Studi, Trieste, Italy*

(Received: 31 January 2023; accepted: 7 August 2023; published online: 29 September 2023)

ABSTRACT The Mediterranean Sea area is an important region of the world and the knowledge of its characteristics is crucial not only for scientific but also industrial purposes, like guiding companies towards an optimal exploitation of the available resources in the area. Over the years, many research institutions, as well as private companies, have performed seismic campaigns aimed at inferring the characteristics and principal features of the crust in this region. By analysing the scientific literature on the area, many data sets, in the form of maps, interpreted seismic profiles or scattered data, that model small regions of the Mediterranean Sea area, mainly in terms of depths of geological horizons, can easily be retrieved. What is actually hard to find is comprehensive information on the entire Mediterranean Sea area. In this framework, the principal purpose of this work is to exploit all data sets, retrievable in literature, that model the main geological horizons of various parts of the Mediterranean Sea area and combine them with the aim of obtaining a full 3D model covering the whole region. The idea is to build a 3D model, completed by the density and magnetic susceptibility distributions, and an estimate of its accuracy.

Key words: Mediterranean Sea, geophysical data combination, 3D crustal model, gravity field analysis, magnetic field analysis.

1. Introduction

The Mediterranean Sea is made up of several basins characterised by different morphologies, crustal types and ages. This complex setting has been produced by tectonic movements, related to the convergence of the African and Eurasian plates, which occurred over the past millions of years and is still currently active. For example, the basins of the eastern Mediterranean contain traces of a slow continental subduction process of the African plate below the Eurasian (Le Pichon and Angelier, 1979), while the Calabro-Sicilian arc displacement towards SE led to the formation of the Tyrrhenian Sea, characterised by the presence of oceanic crust (Savelli and Ligi, 2017). The western Mediterranean oceanic basin was formed following the separation of the Corsica-Sardinia arc from Europe (Gueguen *et al.*, 1998). A significant consequence of the collision between the African and European plates was the reduction of water inflows into the Mediterranean Sea in the Late Miocene, leading to the geological event generally referred to as the Messinian salinity crisis (Krijgsman *et al.*, 1999). A consequence of such reduced inflows was, in fact, an unbalanced evaporation process, which led to the formation of salt deposits of different thicknesses in the deep basins in the entire Mediterranean region (Hsü *et al.*, 1973; Sonnenfeld, 1985; Lofi, 2018). The subsequent halokinetic tectonic movements produced

salt structures reaching up to 3 km in thickness. Over the years, many geophysical campaigns have been conducted in the Mediterranean Sea region to unveil the wide variety of basins and morphological units (of different ages and with different features) to better understand the geological evolution processes. Oil companies, for example, with their interest in exploring and exploiting natural resources, have performed various seismic campaigns with the purpose of investigating deep structures to retrieve new potential reservoirs.

In literature, it is possible to retrieve a large amount of various information about the Mediterranean Sea, ranging from interpreted seismic profiles (e.g. Ben-Avraham *et al.*, 2002; Finetti, 2003; Makris and Yegorova, 2006; Longacre *et al.*, 2007; Feld *et al.*, 2017; d'Acremont *et al.*, 2020; Bellucci *et al.*, 2021) to local maps on sediments, such as Messinian evaporites (e.g. Carton *et al.*, 2009; Güneş *et al.*, 2018), as well as regional models on the basement and Moho (e.g. Fullea *et al.*, 2021; Gard and Hasterok, 2021). The fairly scant information on the entire Mediterranean region consists of the maps developed within the International Bathymetric Chart of the Mediterranean (IBCM), an intergovernmental project in which, apart from the depth maps of the shallower layers (e.g. the thickness of the Plio-Quaternary sediments), regional gravity and magnetic maps (IOC, 1981) are also available. What is missing in the reference literature is complete information on deeper layers up to the Moho, expressed not only in terms of surfaces, but also in terms of density distribution or magnetic properties of the crustal layer. In this framework, the scope of this work is to provide a full 3D model of the principal geological horizons (corresponding to the crustal density discontinuity surfaces), densities and susceptibilities, which would represent a significant update and improvement of the IBCM products. The objective is to collect all freely available information in the form of interpreted seismic profiles, well logs, local maps and geological characterisations of the main units, and combine them to obtain a homogeneous 3D model. Starting from the analysis of the scientific documents, once the main layers to be modelled have been defined, the literature research focused on retrieving as much information as possible on them and, then, we applied an interpolation by means of kriging to merge all the data together. In this way, the kriging interpolation has provided not only the prediction of our modelled horizons on a regular grid given a set of sparse points, but it has also enabled estimating the prediction error, which can be useful to evaluate the expected reliability of the 3D model for future applications. In other words, the prediction error can be considered an estimate of the confidence of the results and it is basically the uncertainty, expressed as a standard deviation that can be associated to the interpolation result. The Mediterranean area is modelled as a 3D volume composed of voxels with a spatial resolution of approximately 15 km x 15 km and a vertical resolution of about 300 m up to a depth of 45 km. In the next sections, the data used to estimate the depths of the main geological horizons of our model will be presented together with information on density and magnetic susceptibility. Ultimately, the resulting 3D model will be discussed with an analysis of the most accurate gravity and magnetic observations over the area to draw preliminary considerations on the modelled crustal features.

2. Geological layers

All data on the geological units of the Mediterranean Sea, including interpreted seismic profiles and compiled maps, freely available in literature, were collected in this work. These data have been used to produce the 2D depth maps of the main geological layers, corresponding to the crustal density discontinuity horizons such as, for example, the topography/bathymetry,

the base of Plio-Quaternary sediments and Messinian evaporites, the basement, and Moho. Next, the Curie isotherm depth, the reference surface below which the materials are no longer magnetised, has also been investigated and modelled. All the modelled layers are shown in Fig. 1 together with the estimate of their corresponding accuracy. A description of the data used for each single horizon is presented in the following.

The bathymetry depth has been retrieved from the Etopo1 model (Amante and Eakins, 2009). Considering that this layer is currently known with a high level of accuracy, its geometries have been considered exact, meaning that its uncertainty was assumed to be equal to zero. Even if this is not entirely true, it is justified by the fact that at the chosen spatial and vertical resolutions of about 15 km and 300 m, used for our modelling, it is certainly the best known layer and it is realistic to presume its uncertainty to be negligible, its error being at least one order of magnitude smaller than the model resolution (Sun *et al.*, 2021).

The depth of the bottom of the Plio-Quaternary sediments has been obtained by summing the Plio-Quaternary sediment thickness (derived from Capponi *et al.*, 2020), which was estimated from a digitised version of the IBCM-PQ map (IOC, 1981) integrated with seismic interpreted profiles, to the bathymetry map. Within Capponi *et al.* (2020), a formal accuracy ranging between 100 and 200 m has also been estimated. This information is used to set the corresponding uncertainty of our modelled layer at ± 150 m.

In order to model the subsequent geological horizon (i.e. the depth of the base of the Messinian evaporites), the thickness of the evaporites taken from the regional map of Haq *et al.* (2020) and the sparse thickness values, derived from the seismic profiles interpreted by de Voogd *et al.* (1992), Ben-Avraham *et al.* (2002), Finetti (2003), Makris and Yegorova (2006), Longacre *et al.* (2007), Feld *et al.* (2017), d'Acremont *et al.* (2020), and Bellucci *et al.* (2021), have been merged together by means of a kriging interpolation (Wackernagel, 2003). Apart from the map from Haq *et al.* (2020), which covers the whole Mediterranean region, the seismic profiles used to build the depth of the base of the Messinian evaporites are spread all over the Mediterranean Sea, as shown in Fig. 2, and are mainly concentrated in the easternmost part.

Since all the data from the abovementioned literature were available only as published images, the first step was to geo-reference and digitise them starting from the thickness map from Haq *et al.* (2020), and, then, proceed with each seismic profile (i.e. all the profiles shown in Fig. 2), so as to obtain the digitised version of the data set. The result of this operation is a thickness map and a set of thickness values along the various profiles of the Messinian geological layer. Among the used interpreted seismic profiles, not all of them were given as depths so, for those provided in terms of two way travel times (TWT), the digitised map from Haq *et al.* (2020) - in particular its corresponding values at the location of the interested profile - was used to determine the proper conversion factor to convert from TWT to depths. At this point, the empirical variogram was computed from the data and fitted with a Stable variogram function. Next, by applying ordinary kriging (Wackernagel, 2003) to all the digitised data, the final grid of the Messinian thickness and its corresponding error (i.e. the kriging prediction error) was obtained. Ultimately, to convert this layer base from thickness to depth, the thickness considered must be summed to the depth of the base of the Plio-Quaternary sediments. From the ordinary kriging interpolation, a relative accuracy, ranging between ± 300 and ± 500 m, was obtained for this layer.

The deeper geological horizon is the basement, namely the boundary surface between the Pre-Messinian sediments and the crystalline crust. A unique geological unit for the pre-Messinian sediments was hypothesised due to the lack of detailed information about the different deep sedimentary packs over several areas of the Mediterranean region. In fact, standard seismic acquisitions do not reach the depths necessary to accurately see and model these layers and,

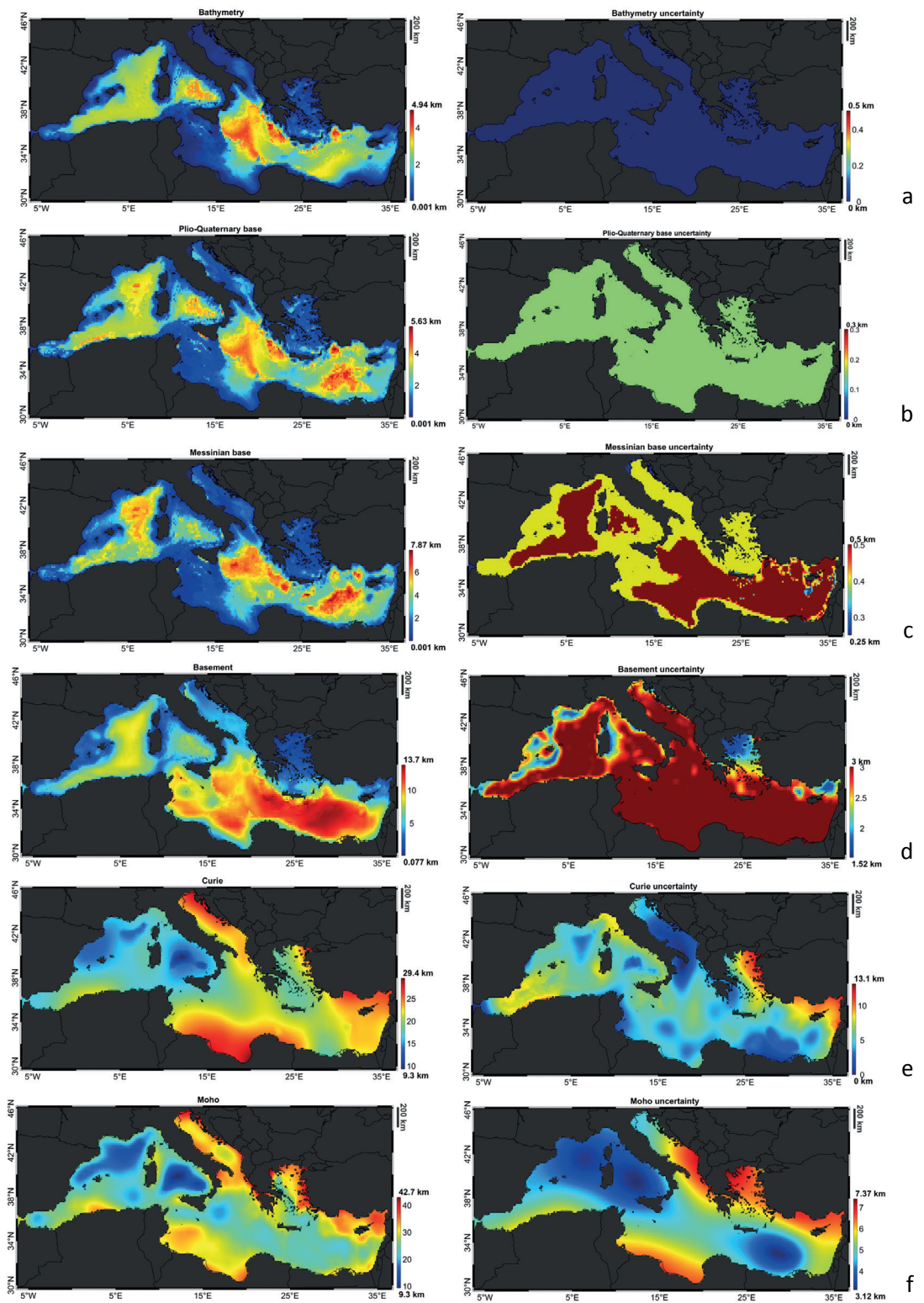


Fig. 1 - Geological horizons (left column) and their corresponding accuracy (right column), in the following order: bathymetry (a), base of Plio-Quaternary sediments (b), base of Messinian evaporites (c), basement (d), Curie isotherm (e) and Moho (f).

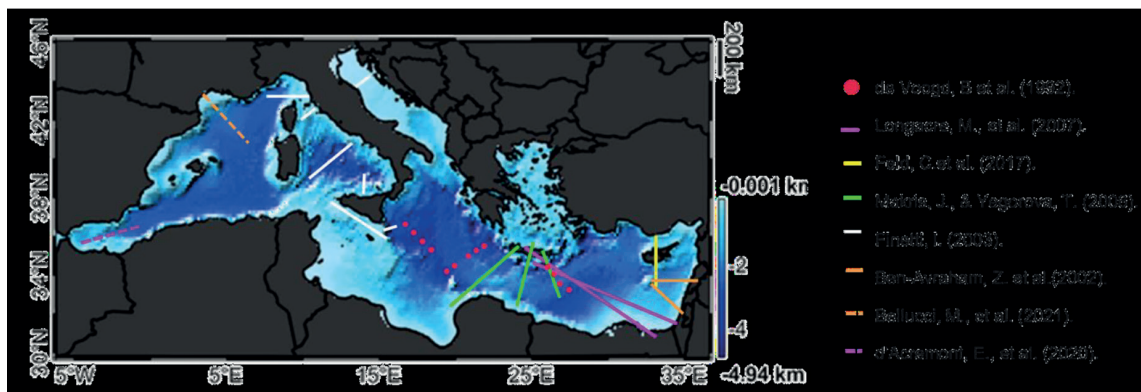


Fig. 2 - Interpreted seismic profile location used in addition to the map from Haq *et al.* (2020), to produce the depth map of the Messinian evaporites; different colours for the profile positions refer to different publications, according to the legend.

consequently, only a few deep seismic profiles are available (and are not sufficient for a proper detailed modelling of the whole Mediterranean). Moreover, the different pre-Messinian sediments have very similar densities, thus making the definition of a clear boundary between them a difficult task (Saleh, 2013). For all these reasons, the bottom of this layer, i.e. the basement (or top of the crystalline crust), was directly modelled, exploiting the global sediment thickness model by Straume *et al.* (2019). It was interpolated over our grid and, then, by summing it to the bathymetry, the depth to the basement was retrieved. Since the source for this layer is a global model, and given the absence of better refined information, a ± 3 -kilometre uncertainty was assigned to this horizon. This value corresponds to a relative error of about 20% in standard deviation (STD), larger than the ones estimated for the shallower sediments and evaporites in the order of 10% in STD.

The Moho depth and its accuracy have been drawn from the European model by Grad *et al.* (2009), and the model has simply been reinterpolated over our grid.

The last modelled horizon is the Curie isotherm, which is the surface identifying the Curie Point depth, namely the theoretical surface with a temperature of approximately 580 °C that can be considered the bottom of magnetic sources (above Curie temperature ferromagnetic minerals are converted to paramagnetic minerals). The definition of a Curie depth map is not a simple task, since no regional models are available in literature. Besides global models (Li *et al.*, 2017; Gard and Hasterok, 2021), that present large differences in the Mediterranean Sea area (about 6 km in terms of STD) in any case, only a few local models are available, e.g. on the Iberian peninsula (Andrés *et al.*, 2018) or close to the Egyptian coastline (Elbarbary *et al.*, 2018). For this work, the Li *et al.* (2017) Curie isotherm was selected, but due to the large discrepancies with the other models, it was assigned a high uncertainty of ± 7 km. The high uncertainty of this surface finds confirmation in the comparison between the Li *et al.* (2017) model and the Curie isotherm derived from the WINTERC-g model, where differences up to 23 km were retrieved (see the two models in Fig. 3). A possible explanation of these large differences could be related to the fact that the Curie Point depth estimation is generally performed by exploiting the relationship between the spectrum of magnetic anomalies and magnetic source depth (Blakely, 1996), without a proper modelling of the actual distribution of the real magnetic susceptibility. Looking at the two models in Fig. 3, we note that the 6-kilometre uncertainty is very close to the actual STD of the Curie isotherm undulation, thus confirming how poor the availability of knowledge on this surface actually is.

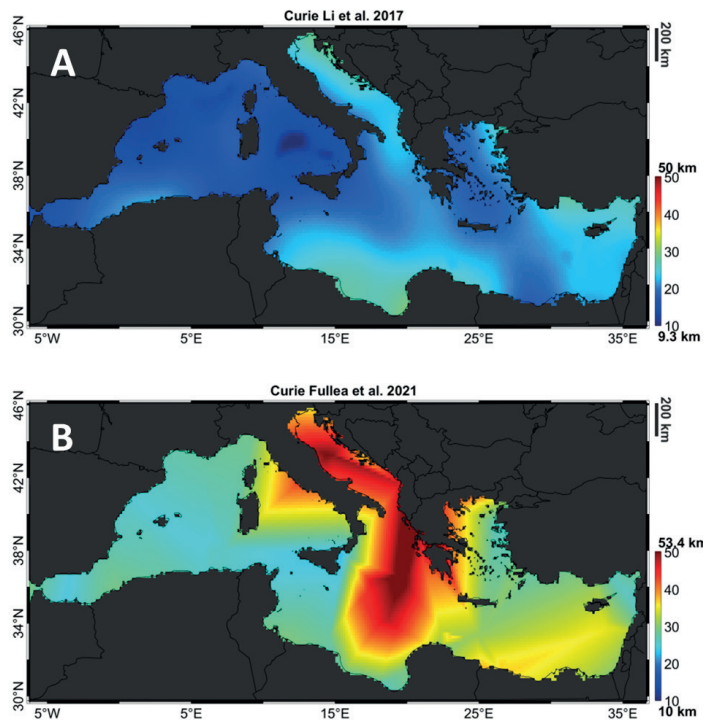


Fig. 3 - The Curie isotherm from Li *et al.* (2017) (A) and interpolated from the WINTERC-G model (B).

At this point, once all the geological horizons have been set and defined, in order to homogenise the data, and with the idea of building a full 3D model, starting from the shallowest layers, we adjusted the deeper horizons in order to avoid intersection between them. This procedure was applied to avoid unrealistic scenarios, such as, for example, the Moho rising above the basement or the basement rising above the bathymetry (events which would certainly never occur), that, in principal, could have occurred due to the different sources used to model the layers in this work. For the Curie isotherm, which in a few small areas was descending below the Moho (allowing, in principle, to also obtain a magnetised mantle), we chose to modify it in such a way as to always let it fall within the basement and Moho. In other words, in our modelling we assumed the crust to be the only geological layer with magnetised/unmagnetised features. This choice is motivated by the fact that the Curie isotherm is probably the most uncertain layer and that, by neglecting the magnetised part of the upper mantle, it is admissible in a model on such a large scale.

3. Densities and magnetic susceptibility distributions

In order to complete the 3D model, once all the geological layers have been defined, information is needed on the density and magnetic susceptibility for each of the geological units that will be used to assign a density/susceptibility value to all the voxels of the 3D volume of this work. A simple method for obtaining such information consists in defining, for each layer, the principal characteristics of the density and susceptibility models in terms of mean density/susceptibility values and vertical gradients for density/susceptibility (in terms of density, the latter are useful to simulate compaction processes). By also adding the STD, information about the accuracy of the

model of this paper is provided. Table 1 shows the values used to model the density distribution in the study area. In detail, standard mean density values, with null vertical gradients, and STD values were used for the shallowest layers (water, Plio-Quaternary sediments, and Messinian evaporites) to obtain reasonable density variations according to standard geological knowledge. It is worth observing, assuming that our density/susceptibility distributions for each element of our 3D volume are normally distributed with a mean given by the mean value and a variance given by the square of the STD, that we can expect density/susceptibility variations in the range of ± 3 STDs. For example, for the Plio-Quaternary sediments the density of our model can range between 2,130 and 2,270 kg/m³, a range consistent with the work by Montone and Mariucci (2015). As the Messinian evaporites are mainly composed of gypsum and salt (Haq *et al.*, 2020), a mean density, equivalent to that of halite (Ellis and Singer, 2007), was set assuming variations ranging between 2,128 and 2,212 kg/m³. In the pre-Messinian sediments, the mean value was taken from the CRUST1.0 sedimentary layer (Laske *et al.*, 2013), and a vertical gradient of 7 kg/m³/km was also introduced to simulate sediment compaction (with this gradient, vertical density variations, from 2,400 kg/m³, at zero level, to 2,520 kg/m³, at 17 km of depth, were modelled). The range of variability for this unit of sediments was set in order to admit density values equal to the maximum density of CRUST1.0. For the crystalline crust, given that large variations in the density distribution (due to different crustal domains) are quite common, especially in the complex Mediterranean area, the decision fell upon using a more refined density model taken from Fullea *et al.* (2021), with spatial lateral variations having, in return, an average density of 2,890 kg/m³. For the mantle, we used a density model from Hunt *et al.* (1995) in which the average upper mantle density was approximately 3,321 kg/m³. For both the crust and upper mantle, the STD was set to 32 kg/m³, leading to their densities having a large range of variability, approximately ± 100 kg/m³.

Table 1 - Average density, vertical linear gradient and accuracy values for each modelled geological layer.

| | Average Density [kg/m ³] | Vertical density gradient [kg/m ³ /km] | Density accuracy [kg/m ³] |
|-----------------|--------------------------------------|---------------------------------------------------|---------------------------------------|
| Water | 1,030 | 0 | 0 |
| Plio-Quaternary | 2,200 | 0 | 22.4 |
| Messinian | 2,170 | 0 | 14 |
| Pre-Messinian | 2,400 | 6 | 26.5 |
| Crust | 2,890* | 6 | 32 |
| Mantle | 3,321* | 0 | 32 |

* The crust and upper mantle density distributions are not uniform inside the layers but are variable, taken from Hunt *et al.* (1995) and Fullea *et al.* (2021), respectively.

Table 2 shows the values used for the susceptibility distribution. Information on susceptibility is not easy to retrieve and, when available, is characterised by considerably greater variability [see the works of Telford *et al.* (1990), Mancinelli *et al.* (2015), and Lowrie and Fichtner (2020)]. Water and evaporates are the only exceptions, as their susceptibility is well known. This is reflected in our model where they were assigned a very low variability of -13×10^{-6} SI and -30×10^{-6} SI. For the Plio-Quaternary and pre-Messinian sediments, the mean susceptibility values and the STD were selected based on the work of Hunt *et al.* (1995). With regards to the crystalline crust

layer, the choice was made to use the very smooth model by Hemant and Maus (2005), with very high uncertainty, in which susceptibility can range between extremely low values, around 0 SI (typical for continental domains), and about 0.06 SI, generally associated with basaltic rocks and gabbroids. For the upper mantle, being below the Curie isotherm, we obviously assumed zero susceptibility. It is worth noting that, within the current work, we have not modelled the remanent magnetisation, as we assumed that it would affect the magnetisation in particularly localised areas and, in a large scale regional study such as this, these effects could be neglected. This reasoning is also confirmed by the global-scale study by Hemant and Maus (2005) that presents low remanent magnetisation values in the Mediterranean Sea.

Table 2 - Magnetic susceptibility average values, vertical linear gradient and accuracy for each modelled geological layer.

| | Average Susceptibility [10^{-6} SI] | Vertical susceptibility gradient [10^{-6} SI /km] | Susceptibility accuracy [kg/m^3] |
|-----------------|----------------------------------------|------------------------------------------------------|---------------------------------------------|
| Water | -13 | 0 | 10 |
| Plio-Quaternary | 200 | 0 | 63 |
| Messinian | -30 | 0 | 10 |
| Pre-Messinian | 900 | 0 | 150 |
| Crust | 19,709* | 0 | 11,662 |
| Mantle | 0 | 0 | 0 |

* The crustal susceptibility values are taken from Hemant and Maus (1995).

At this stage, by exploiting all this density and susceptibility information, it is possible to fill the full 3D volume and build the equivalent density/susceptibility 3D distributions.

In Fig. 4, the 3D model is reported in terms of geological layers, density, and magnetic susceptibility distributions. The volume is cut at latitude 36° N to show interesting details in terms of density/susceptibility distributions. In particular, the first cube (Fig. 4A) represents the geometries of our modelled horizons, where each label value corresponds to a geological unit, i.e. 1 = water, 2 = Plio-Quaternary sediments, 3 = Messinian evaporites, 4 = pre-Messinian sediments, 5 = magnetised crystalline crust, 6 = unmagnetised crystalline crust, 7 = upper mantle. In the density distribution (Fig. 4B), the crust and upper mantle, where the horizontal density variations are clearly visible, are highlighted. By observing the susceptibility distribution (Fig. 4C), the crust results to be the main magnetised geological layer and, within it, the differences between the crustal oceanic domains (high magnetic susceptibility values) and continental domains (low magnetic susceptibility values) can also be observed.

Fig. 5 shows an example of a profile that can be obtained from the resulting 3D volume. In particular, the two sections show the density and magnetic susceptibility distributions, respectively. It can be noted that, in correspondence of the central Mediterranean Sea (Speranza *et al.*, 2012), characterised by the oceanic crustal domain of the Ionian basin, the density section shows the typical thinning of oceanic crust due to a shallower Moho and high crustal density values, whereas the increase of magnetisation is evident in the susceptibility section, that only represents the magnetised part of the crust.

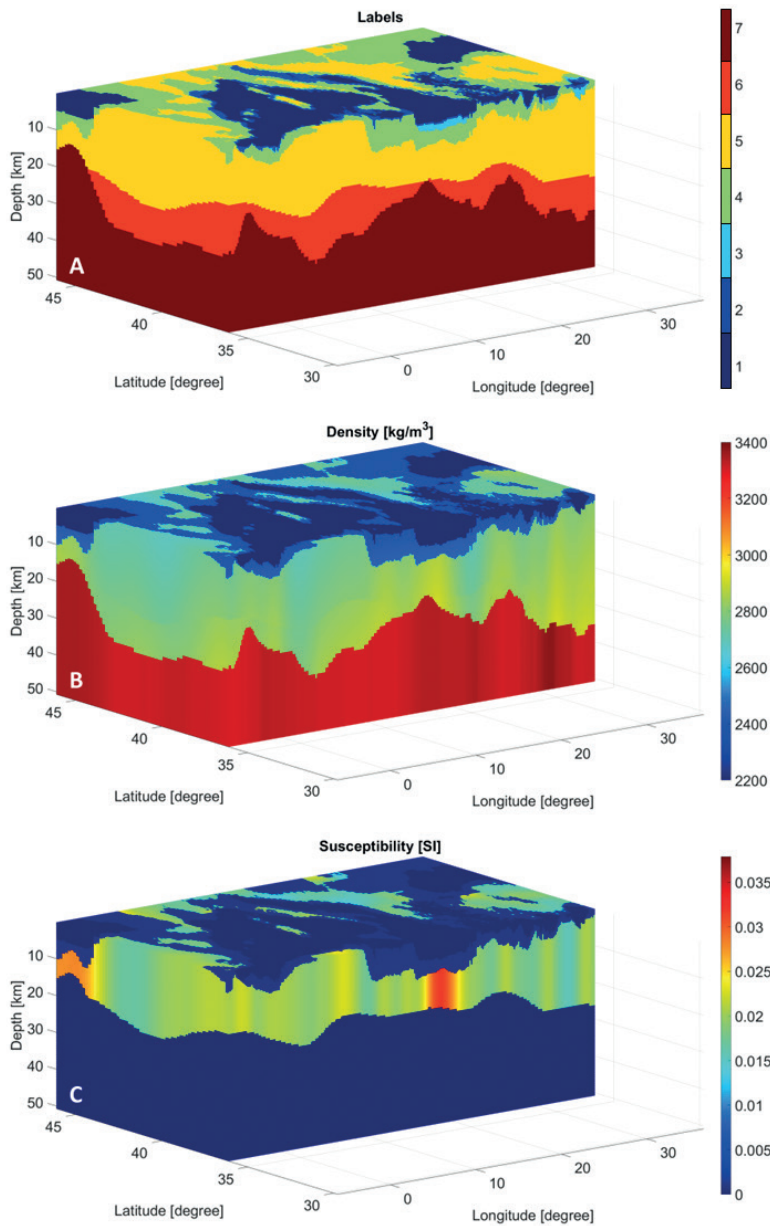


Fig. 4 - Resulting 3D model of the Mediterranean Sea expressed in terms of geological layers (A), density with unit (kg/m³) (B) and magnetic susceptibility with unit (10⁻⁶ SI) (C).

4. Gravity and magnetic observations

Once the 3D model of the area has been completely defined, we performed a harmonic synthesis of the gravity observations from the XGM2019e model by Zingerle *et al.* (2020), by exploiting the spherical harmonic coefficients up to the degree/order of 2,190, on a grid with the same planar coordinates of our volume at an altitude of 1,500 m a.s.l. (to be outside the masses). The maximum degree/order of the spherical harmonic coefficients (i.e. 2,190) was chosen to have a gravity signal with a spatial resolution of the same order of magnitude as our modelled volume, i.e. 15 km × 15 km (Fig. 6). Gravity disturbances were used, and the topography and bathymetry effects, computed from Rexer *et al.* (2017), were removed from them in order to

Fig. 5 - Example of two sections in terms of density (II) and magnetic susceptibility (III) from the 3D model of the Mediterranean Sea. Panel I is the bathymetry map with the white line showing the location of the displayed profile.

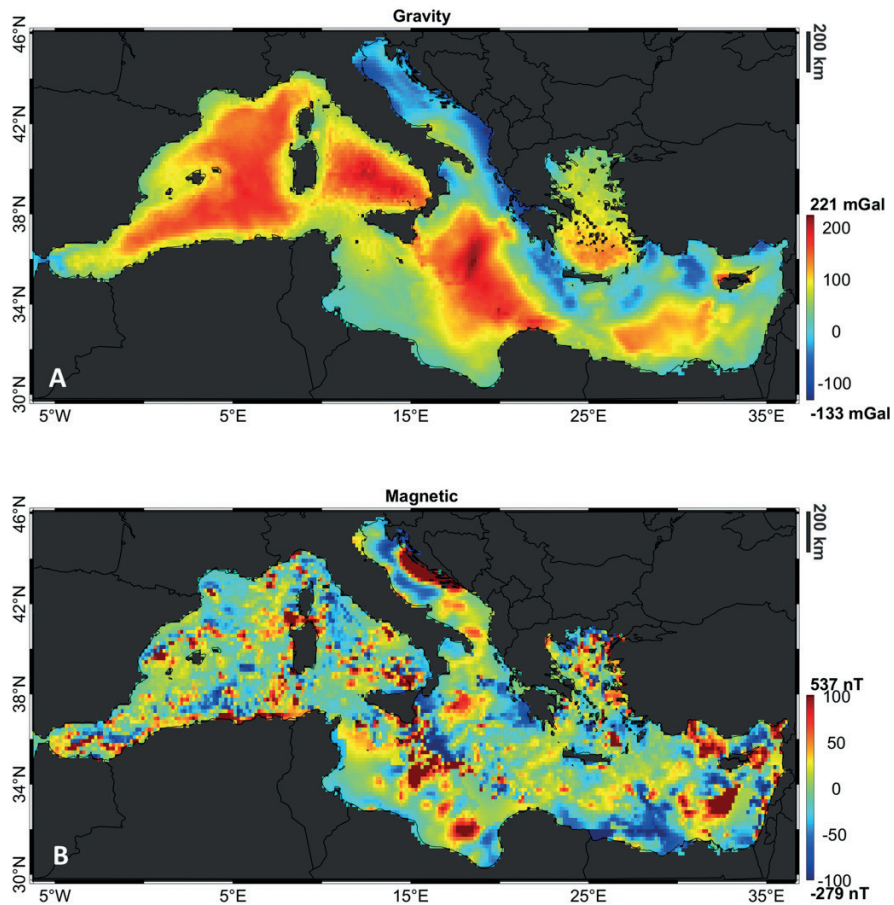
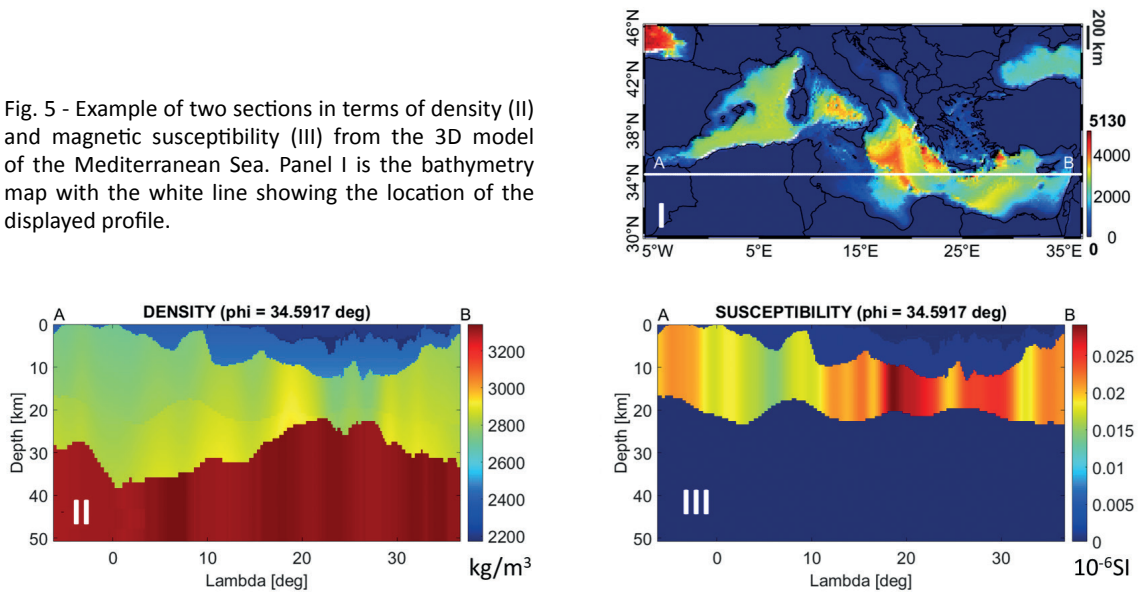


Fig. 6 - Reduced gravity disturbance (A) and magnetic anomaly (B) observations, respectively from the XGM2019e global gravity model and EMAG2v3 model.

enhance signals due to deeper structures. It is worth recalling that gravity disturbance is defined as the difference between the actual gravity at a given point and the normal gravity at the same point [for further theoretical details, refer to Hofmann-Wellenhof and Moritz (2006) and Barthelmes (2009)]. Since our model reaches a depth of 50 km, the gravitational effect of a density distribution model between 50 and 300 km, drawn from the work of Fulla *et al.* (2021), was also removed from the observations. The 300-kilometre depth for this further reduction has been defined according to the works of Sampietro and Capponi (2019) and Sampietro *et al.* (2023). An important remark should be made on the accuracy of the XGM2019e model and, more in general, of these kinds of global models. This is a complex matter to evaluate as it mainly depends on the availability of high resolution and accurate gravity data used to build the model itself, as well as on the spectral characteristics of the local gravitational field. For the purposes of this study, this problem was simplified by comparing the XGM2019e gravity disturbances with ground data on the study area [available from the International Gravimetric Bureau by Drewes *et al.* (2016)] and obtaining a STD for the differences of about 2.7 mGal. For this reason, the gravity data was assumed to have an accuracy of 3 mGal.

As for the magnetic observations, the EMAG2v3 global magnetic anomaly map by Meyer *et al.* (2017) was selected and interpolated on a grid with the same planar coordinates of the gravity observations, at an altitude of 4,000 m a.s.l. The accuracy of the magnetic data is assumed to be about 23 nT in terms of STD error, according to Sampietro *et al.* (2023) in which it was evaluated by exploiting other independent data sets. Once the potential field observations were defined, an attempt was made to evaluate the consistency of our 3D geological model with the observed fields. Therefore, we applied the forward computation method, by computing the residuals both in terms of gravity and magnetic anomaly, i.e. the differences between the observed signals and the gravity and magnetic forwards of our 3D model (Fig. 7). By observing the gravity residuals, it

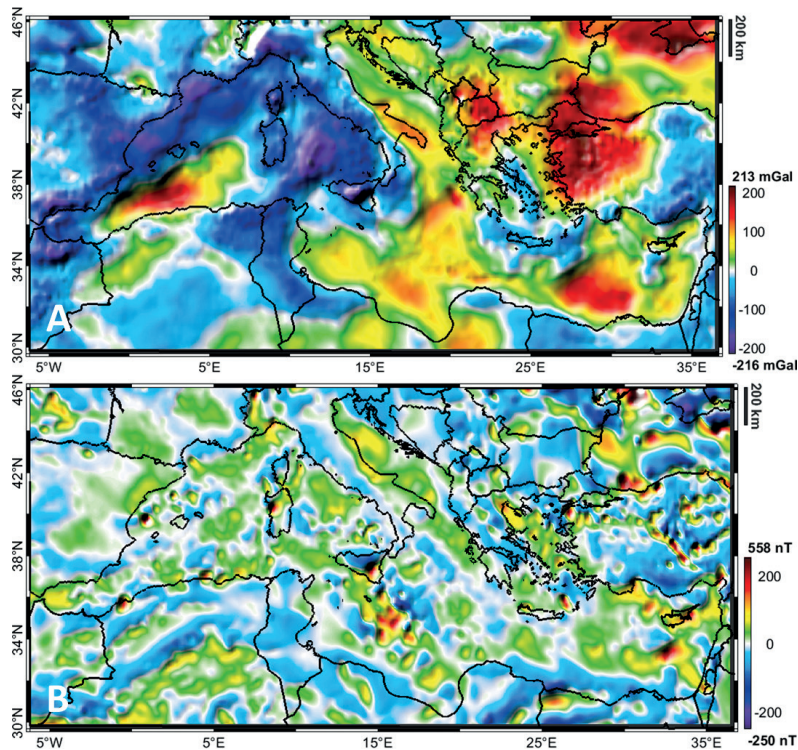


Fig. 7 - Gravity (A) and magnetic (B) residuals computed as differences between the observed fields and the effects evaluated from the 3D model by means of forward operator.

can be noted that they are even larger than the observed signals (73 mGal vs. 69 mGal in terms of STD) with negative values in the western Mediterranean Sea and positive values in the central-eastern Mediterranean Sea. These differences can mainly be associated to mismodelling in the crustal density distribution. By analysing these residuals, it is possible to actually infer where the 3D model is lacking mass or has a surplus of mass, thanks to the positive or negative sign of the residuals, respectively. Similar observations can also be made for the magnetic field, where the residuals are slightly higher than those in the observed field (STD of 51 nT vs. 58 nT). Again, in this case the main effect is probably in the magnetic susceptibility of the crust, namely the layer that principally affects the observed magnetic field.

5. Conclusions

The complex history of the Mediterranean Sea has led to the formation of several basins with highly different characteristics. This has made the Mediterranean Sea one of the most interesting areas to be studied, both for scientific and industrial purposes. Over the last decades, many data have been collected and various regional/local studies have been carried out. The aim of this work is to define a comprehensive data set of the main geological horizons, publicly available to the community. For this reason, all the freely retrievable data sets on the Mediterranean Sea were collected and integrated in order to obtain a homogeneous data set expressed as depths of the principal geological horizons, corresponding to the crustal density discontinuity surfaces. Moreover, we tried to define a full 3D model for the density and magnetic susceptibility distributions by integrating the sparse information available on the geological characteristics of the layers. A considerable effort was made to provide not only the data set and 3D model, but also a quantitative evaluation of its expected accuracy, which is an extremely important piece of information for a proper future use of the data and for the analysis of its reliability.

Ultimately, once the model was realised, we also performed a first check of the match between the observed gravity and magnetic signals with the signals obtained by applying the forward operator to our model. From the analysis of the residuals, in both cases the mismatch with the observed field proved to be quite large, and in the most complex areas, there were features that should have been modelled with more details, because they presented an excess or lack of masses (in relation to gravity) or different magnetic sources. In the near future, the gravity and magnetic data inversion would represent the following step required to improve and refine the model, which integrates all the information freely available in literature, in order to obtain a result that is not only realistic but also in agreement with the observed potential fields. This next step is one of the objectives of the XORN project, funded by the European Space Agency, within which the present work falls. However, the 3D model provided can be considered an improvement with respect to the state of the art in the Mediterranean Sea and also represents a starting point for other geophysical studies, on a regional and local scale. The 3D model presented in this work will be freely made available to the community upon request to the authors.

REFERENCES

- Amante C. and Eakins B.W.; 2009: *ETOPO1 arc-minute global relief model: procedures, data sources and analysis*. National Oceanic and Atmospheric Administration (NOAA), Boulder, CO, USA, Technical Memorandum NESDIS NGDC-24, 22 pp., doi: 10.7289/V5C8276M.
- Andrés J., Marzán I., Ayarza P., Martí D., Palomeras I., Torné M., Campbell S. and Carbonell R.; 2018: *Curie point depth of the Iberian peninsula and surrounding margins: a thermal and tectonic perspective of its evolution*. *J. Geophys. Res.: Solid Earth*, 123, 2049-2068.

- Barthelmes F.; 2009: *Definition of functionals of the geopotential and their calculation from spherical harmonic models: theory and formulas used by the calculation service of the International Centre for Global Earth Models (ICGEM)*. Deutsches GeoForschungsZentrum GFZ, Potsdam, Germany, Scientific Technical Report STR09/02, 35 pp., doi: 10.2312/GFZ.b103-0902-26, < icgem.gfz-potsdam.de >.
- Bellucci M., Pellen R., Leroux E., Bache F., Garcia M., Do Couto D., Raad F., Rabineau M., Gorini C., Moulin M., Maillard A., Lofi J., Del Ben A., Camerlenghi A., Poort J. and Aslanian D.; 2021: *A comprehensive and updated compilation of the seismic stratigraphy markers in the western Mediterranean Sea*. SEANOE, Plouzane, France, 10 pp., doi: 10.17882/80128.
- Ben-Avraham Z., Ginzburg A., Makris J. and Eppelbaum L.; 2002: *Crustal structure of the levant basin, eastern Mediterranean*. *Tectonophys.*, 346, 23-43.
- Blakely R.J.; 1996: *Potential theory in gravity and magnetic applications*. Cambridge University Press, Cambridge, UK, 441 pp.
- Capponi M., Glavich E. and Sampietro D.; 2020: *Map of Plio-Quaternary sediment depths in the Mediterranean Sea*. *Boll. Geof. Teor. Appl.*, 61, 421-432.
- Carton H., Singh S.C., Taponnier P., Elias A., Briaes A., Sursock A., Jomaa R., King G.C.P., Daeron M., Jacques E. and Barrier L.; 2009: *Seismic evidence for Neogene and active shortening offshore of Lebanon (Shalimar cruise)*. *J. Geophys. Res.: Solid Earth*, 114, B07407, 26 pp., doi: 10.1029/2007JB005391.
- d'Acremont E., Lafosse M., Rabaute A., Teurquety G., Do Couto D., Ercilla G., Juan C., de Lépinay B.M., Lafuerza S., Galindo-Zaldivar J., Estrada F., Vazquez J.T., Leroy S., Poort J., Ammar A. and Gorini C.; 2020: *Polyphase tectonic evolution of fore-arc basin related to STEP fault as revealed by seismic reflection data from the Alboran Sea (W-Mediterranean)*. *Tectonics*, 39, e2019TC005885, 25 pp., doi: 10.1029/2019TC005885.
- de Voogd B., Truffert C., Chamot-Rooke N., Huchon P., Lallemand S. and Le Pichon X.; 1992: *Two-ship deep seismic soundings in the basins of the eastern Mediterranean Sea (Pasiphae cruise)*. *Geophys. J. Int.*, 109, 536-552, doi: 10.1111/j.1365-246X.1992.tb00116.x.
- Drewes H., Kuglitsch F.G., Adám J. and Rózsa S.; 2016: *The geodesist's handbook 2016*. *J. Geod.*, 90, 907-1205, doi: 10.1007/s00190-016-0948-z.
- Elbarbary S., Zaher M.A., Mesbah H., El-Shahat A. and Embaby A.; 2018: *Curie point depth, heat flow and geothermal gradient maps of Egypt deduced from aeromagnetic data*. *Renewable Sustainable Energy Rev.*, 91, 620-629.
- Ellis D.V. and Singer J.M.; 2007: *Well logging for Earth scientists, 2nd ed.* Springer, Dordrecht, The Netherlands, 706 pp.
- Feld C., Mechie J., Hübscher C., Hall J., Nicolaidis S., Gurbuz C., Bauer K., Loudon K. and Weber M.; 2017: *Crustal structure of the Eratosthenes Seamount, Cyprus and s. Turkey from an amphibian wide-angle seismic profile*. *Tectonophys.*, 700, 32-59, doi: 10.1016/j.tecto.2017.02.003.
- Finetti I.R.; 2003: *The CROP profiles across the Mediterranean Sea (Crop Mare I and II)*. *Mem. Descr. Carta Geol. It.*, LXII, 171-184.
- Fullea J., Lebedev S., Martinec Z. and Celli N.; 2021: *Winterc-G: mapping the upper mantle thermochemical heterogeneity from coupled geophysical-petrological inversion of seismic waveforms, heat flow, surface elevation and gravity satellite data*. *Geophys. J. Int.*, 226, 146-191, doi: 10.1093/gji/ggab094.
- Gard M. and Hasterok D.; 2021: *A global Curie depth model utilising the equivalent source magnetic dipole method*. *Phys. Earth Planet. Inter.*, 313, 106672, 34 pp., doi: 10.1016/j.pepi.2021.106672.
- Grad M., Tiira T. and Group E.W.; 2009: *The Moho depth map of the European plate*. *Geophys. J. Int.*, 176, 279-292.
- Gueguen E., Doglioni C. and Fernandez M.; 1998: *On the post-25 Ma geodynamic evolution of the western Mediterranean*. *Tectonophys.*, 298, 259-269.
- Güneş P., Aksu A.E. and Hall J.; 2018: *Internal seismic stratigraphy of the Messinian evaporites across the northern sector of the eastern Mediterranean Sea*. *Mar. Pet. Geol.*, 91, 297-320.
- Haq B., Gorini C., Baur J., Moneron J. and Rubino J.-L.; 2020: *Deep Mediterranean's Messinian evaporite giant: How much salt?* *Global Planet. Change*, 184, 103052, 14 pp., doi: 10.1016/j.gloplacha.2019.103052.
- Hemant K. and Maus S.; 2005: *Geological modeling of the new champ magnetic anomaly maps using a geographical information system technique*. *J. Geophys. Res.: Solid Earth*, 110, 23 pp., doi: 10.1029/2005JB003837.
- Hofmann-Wellenhof B. and Moritz H.; 2006: *Physical geodesy*. Springer, Vienna, Austria, 420 pp., doi: 10.1007/978-3-211-33545-1.
- Hsü K.J., Ryan W.B. and Cita M.B.; 1973: *Late Miocene desiccation of the Mediterranean*. *Nature*, 242, 240-244.
- Hunt C.P., Moskowitz B.M. and Banerjee S.K.; 1995: *Magnetic properties of rocks and minerals*. Rock physics and phase relations: a handbook of physical constants, American Geophysical Union, Washington, DC, USA, Vol. 3, pp. 189-204, doi: 10.1029/RF003p0189.
- IOC, 1981: *International Bathymetric Chart of the Mediterranean (IBCM)*. UNESCO.
- Krijgsman W., Hilgen F.J., Raffi I., Sierro F.J. and Wilson D.S.; 1999: *Chronology, causes and progression of the Messinian salinity crisis*. *Nature*, 400, 652-655, doi: 10.1038/23231.

- Laske G., Masters G., Ma Z. and Pasyanos M.E.; 2013: *Update on CRUST1.0 - A 1-degree global model of Earth's crust*. In: Proc. EGU General Assembly, Vienna, Austria, Geophys. Res. Abstr., Vol. 15, p. 2658.
- Le Pichon X. and Angelier J.; 1979: *The Hellenic arc and trench system: a key to the neotectonic evolution of the eastern Mediterranean area*. Tectonophys., 60, 1-42.
- Li C.-F., Lu Y. and Wang J.; 2017: *A global reference model of Curie-point depths based on EMAG2*. Sci. Rep., 7, 1-9.
- Lofi J.; 2018: *Seismic atlas of the Messinian Salinity Crisis markers in the Mediterranean Sea - Vol. 2*. CCGM and Mémoires de la Société Géologie de France, 181, 72 pp.
- Longacre M., Bentham P., Hanbal I., Cotton J. and Edwards R.; 2007: *New crustal structure of the eastern Mediterranean basin: detailed integration and modeling of gravity, magnetic, seismic refraction, and seismic reflection data*. In: Proc. EGM 2007 International Workshop, European Association of Geoscientists & Engineers, Vol. 15, p. 18, doi:10.3997/2214-4609-pdb.166.D_OP_07.
- Lowrie W. and Fichtner A.; 2020: *Fundamentals of geophysics 3rd ed.* Cambridge University Press, Cambridge, UK, 425 pp., doi: 10.1017/9781108685917.
- Makris J. and Yegorova T.; 2006: *A 3-D density-velocity model between the Cretan Sea and Libya*. Tectonophys., 417, 201-220.
- Mancinelli P., Pauselli C., Minelli G. and Federico C.; 2015: *Magnetic and gravimetric modeling of the central Adriatic region*. J. Geodyn., 89, 60-70, doi: 10.1016/j.jog.2015.06.008.
- Meyer B., Chulliat A. and Saltus R.; 2017. *Derivation and error analysis of the earth magnetic anomaly grid at 2 arc min resolution version 3 (EMAG2v3)*. Geochem., Geophys., Geosyst., 18, 4522-4537, doi: 10.1002/2017GC007280.
- Montone P. and Mariucci M.T.; 2015: *P-wave velocity, density, and vertical stress magnitude along the crustal Po plain (northern Italy) from sonic log drilling data*. Pure Appl. Geophys., 172, 1547-1561.
- Rexer M., Hirt C. and Pail R.; 2017: *High-resolution global forward modelling: a degree-5480 global ellipsoidal topographic potential model*. In: Poster EGU General Assembly, European Geosciences, Vienna, Austria, EGU2017-7725, doi: 10.13140/RG.2.2.29689.26725.
- Saleh S.; 2013: *3D crustal and lithospheric structures in the southeastern Mediterranean and northeastern Egypt*. Pure Appl. Geophys., 170, 2037-2074.
- Sampietro D. and Capponi M.; 2019: *Practical tips for 3D regional gravity inversion*. Geosci., 9, 351, doi: 10.3390/geosciences9080351.
- Sampietro D., Capponi M., Thébault E. and Gailler L.; 2023: *An empirical method for the optimal setting of the potential fields inverse problem*. Geophys. Prospect., 71, 350-365.
- Savelli C. and Ligi M.; 2017: *An updated reconstruction of basaltic crust emplacement in Tyrrhenian Sea, Italy*. Sci. Rep., 7, 18024, 12 pp., doi: 10.1038/s41598-017-17625-2.
- Sonnenfeld P.; 1985: *Models of Upper Miocene evaporite genesis in the Mediterranean region*. In: Stanley D. and Wezel F.C. (eds), Geological Evolution of the Mediterranean basin, Raimondo Selli Commemorative Volume, Springer-Verlag, New York, NY, USA, pp. 323-346.
- Speranza F., Minelli L., Pignatelli A. and Chiappini M.; 2012: *The Ionian Sea: the oldest in situ ocean fragment of the world?* J. Geophys. Res.: Solid Earth, 117, B12101, 13 pp., doi: 10.1029/2012JB009475.
- Straume E.O., Gaina C., Medvedev S., Hochmuth K., Gohl K., Whittaker J.M., Abdul Fattah R., Doornenbal J.C. and Hopper J.R.; 2019: *GlobSed: updated total sediment thickness in the world's oceans*. Geochem., Geophys., Geosyst., 20, 1756-1772, doi: 10.1029/2018GC008115.
- Sun Y., Zheng W., Li Z. and Zhou Z.; 2021: *Improved the accuracy of seafloor topography from altimetry-derived gravity by the topography constraint factor weight optimization method*. Remote Sens., 13, 2277, 18 pp., doi: 10.3390/rs13122277.
- Telford W.M., Geldart L.P. and Sheriff R.E.; 1990: *Applied geophysics*. Cambridge University Press, Cambridge, UK, 770 pp.
- Wackernagel H.; 2003: *Multivariate geostatistics: an introduction with applications 3rd ed.* Springer Verlag, Berlin, Germany, 403 pp., doi: 10.1007/978-3-662-05294-5.
- Zingerle P., Pail R., Gruber T. and Oikonomidou X.; 2020: *The combined global gravity field model XGM2019e*. J. Geod., 94, 66, 12 pp., doi: 10.1007/s00190-020-01398-0.

Corresponding author: Martina Capponi
 Geomatics Research & Development S.r.l.
 Via Cavour 2, 22074 Lomazzo, Italy
 Phone: +39 02 367 14448; e-mail: martina.capponi@g-red.eu